

Deflection of neutral polar molecules using inhomogeneous electric fields

Summer Student Programme 2012

Elizabeth Todd Davies, University of Manchester, United Kingdom

September 2012



Supervisor: Stephan Stern

Centre for Free-Electron Laser Science, DESY, Hamburg, Germany

Abstract

The ability to deflect neutral polar molecules present in supersonic molecular beams using inhomogeneous electric fields is a consequence of these molecules possessing a dipole moment. As a dipole moment is inherently a quantum state-dependent feature, it can thus be exploited to allow spatial separation of neutral molecules in different quantum states. In this report, the Stark interaction was exploited to provide deflection of a gaseous sample of indole (C_8H_7N). Spatial profiles of the molecular beam at various electric field strengths were measured, showing an observed deviation in the beam path attributed to the indole molecules residing in different quantum states. These state-selected samples produced act as ideal samples for laser alignment techniques, in preparation for further experiments such as diffraction on gaseous molecular samples.

Introduction^{1,2}

The fundamental principle, which underpins this experiment, is that neutral polar molecules exhibit a dipole moment. This is imperative for the control of these molecules via deflection in static inhomogeneous electric fields.

The experiment emulated that of the famous Stern-Gerlach experiment of 1922, which showed that individual atoms subjected to an inhomogeneous magnetic field could be spatially separated in accordance with the interaction of their magnetic moment with the field via the *Zeeman effect*¹. In essence, the experiment is a modification upon this important 20th century discovery, with the magnetic field replaced by an electric field, and the separation of states attributed to the *Stark effect*. However, the principle of exploiting the interaction between an atom's dipole moment and an external field, in order to obtain spatial separation of quantum states via deflection in a static field remains unchanged². In an electrostatic field, neutral polar molecules will be deflected by an amount dictated by their dipole moments with molecules in the lowest rotational states being deflected the most as they have greater dipole moments.

This experiment acts as a precursor to laser induced alignment and ultimately to X-ray diffraction experiments, as it leads to the generation of state-selected samples which act as ideal targets for these subsequent experiments. This experiment can be viewed as a calibration experiment, as from analysis of spatial profiles of the deflected molecular beam; one can determine the optimum position to place an alignment laser in order to obtain the maximum alignment possible. As one can choose to select the molecules occupying the low-lying rotational states, which give the greatest response to laser alignment. The highest degree of alignment possible results in an optimized diffraction pattern, with internal structures more easily discerned.

Theory

Stark effect^{1,2,3}

As aforementioned, the ability to deflect neutral polar molecules in strong inhomogeneous electric fields derives itself from the molecule's intrinsic and induced dipole moments. The interaction of the external electric field with the molecule's electric dipole moment induces a perturbation on the atomic energy levels causing separation of the states into $2j+1$ states (where j is the total rotational angular momentum quantum number), resulting in splitting of the molecule's spectral lines¹. This is known as the *Stark effect* with the resulting energy shifts referred to as *Stark shifts*³.

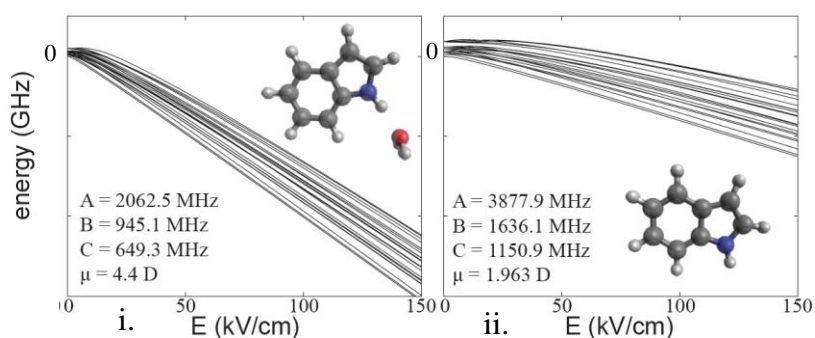


Figure 1: Simulated Stark curves for samples of i. indole(H_2O)₁ and ii. indole₄.

Figure 1 illustrates the Stark shift in energy with increasing external electric field as a result of the Stark interaction for both indole(H_2O)₁ and indole samples. The multiple curves on each graph represent a set of different rotational states of each molecule. As both indole(H_2O)₁ and indole show a decrease in potential energy with increasing electric fields, these molecules are known as high field seeking states (HFS), as they feel a force towards high electric fields. Hence for both molecules a large electric field is energetically favourable. The dipole moment of each rotational state is given by the gradient of the Stark curve, hence from figure 1 it can be inferred that indole(H_2O)₁ has a steeper Stark curve, and as a consequence of this, will have a greater dipole moment.

Principle of Deflection²

The purpose of an *inhomogeneous* electric field (as opposed to a homogeneous field) is to enable deflection of the indole molecules. In a *homogeneous* field the molecules would follow a straight path. However, in an inhomogeneous field the molecules follow a curved path. In this setup, the field is stronger at the top of deflector near the rod (see inset in figure 7), thus as indole molecules are HFS, deflection occurs in the upward direction.

Deflection depends upon the Stark shift, and since the Stark shift is dependent upon the dipole moment of the molecule, it can be inferred that the amount of deflection must also be dependent upon the dipole moment. Hence, the greater the dipole moment (and hence Stark shift), the greater the deflection obtained. Following this logic, from figure 1 it can be seen that the value of the dipole moment varies not only from molecule to molecule, but with the molecule's own rotational state.

The rotational ground state has the largest dipole moment and produces the greatest amount of deflection, whereas the highest rotational state gives the least amount of deflection. The variation of the molecule's dipole moment with the rotational state is important, as the field will cause deflection of each rotational state by varying amounts dictated by the dipole moment of each state, enabling spatial separation of the different quantum states. As low-lying rotational states experience the greatest level of deflection this makes them very appealing for frontier molecular physics experiments including X-ray and electron diffraction of state-selected gaseous molecules.

As the rotational ground state or low-lying states are crucial for these cutting edge experiments, one must have a rotationally cold sample of the order of 1K. Cooling is obtained via supersonic expansion of a molecular sample present within an inert backing gas such as helium². Molecular beams are formed by the expansion of such molecules from a reservoir at high pressure into a region under vacuum by virtue of an orifice⁵.

Indole

Indole (as illustrated in figure 2) is an important molecule, with its properties exploited across a range of industries including the perfume and medical industry, where indole reactions are utilised in drug synthesis processes⁶. The indole nucleus is prevalent within many biological compounds such as serotonin, which is responsible

for the formation of neuron cells and the origin of cognitive processes⁶. Thus experiments investigating indole properties are of great importance to the pharmaceutical industry.

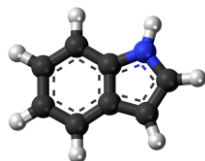


Figure 2: Diagram illustrating the structure of indole⁷.

Experimental Setup and Method

Experimental details and schematics are presented in figures 3-5. In this experiment a dye laser (pumped via a 532nm Nd:YAG laser) was used with a selected wavelength of 283.728 nm (the 1st electronic transition of indole). An Even-Lavie valve providing 20 Hz pulses was also employed, allowing expansion from the gasoline (containing 99.99% He backing gas at approximately 50 bar stagnation pressure and 0.01% vaporized sample of indole held at a few mbar pressure) into the source chamber held at around 10^{-8} mbar, thus providing the cooling of the molecular beam via adiabatic expansion. The backing gas provides the necessary collisions with the indole molecules, with each collision resulting in the removal of the indole molecule's internal kinetic energy (i.e. the vibrational and rotational energies). The energy is transferred to translational velocity carried by He, also adding to the temperature decrease. The inert backing gas is also required to reduce the level of clusters formed after the expansion, which would contribute to heating of the molecular beam and suppress the level of deflection measured⁵. Since the backing gas is non-polar and subsequently has no dipole moment, it will therefore not be deflected; allowing its presence in the sample to be reduced using the skimmers to cut away the undeflected parts of the molecular beam. After multiple collisions between the sample and the backing gas, the sample gas is cooled to ~ 1 K, and the beam is collision-less, with most of the sample populating the rotational ground state or low-lying states.

Each chamber is connected to a turbomolecular pump (TMP) as illustrated in figure 4, in order to maintain vacuum, as some molecules will make contact with the sides of the chamber walls. This would lead to an increase in pressure, and hence an increase in temperature, which is detrimental for deflection measurements as a warm beam implies that the indole sample is not in its rotational ground state. Differential pumping is applied to each chamber as ultra-low pressures are required, thus before the TMPs can be used a rough vacuum must first be generated via the ontol booster.

Skimmers are employed in order to narrow the velocity distribution of the beam. In addition they also collimate the beam before it reaches the deflector plates by cutting away stray rays, so that the beam width is less than the separation of the deflector electrodes. This is necessary as if the beam makes contact with the electrodes, heat will be dissipated and thus the indole molecules will occupy the higher rotational states as opposed to the desired ground state. Skimmers are also advantageous as they reduce the transverse velocity component of the beam, ensuring that the resultant velocity flows almost parallel to the direction of the overall beam flow.

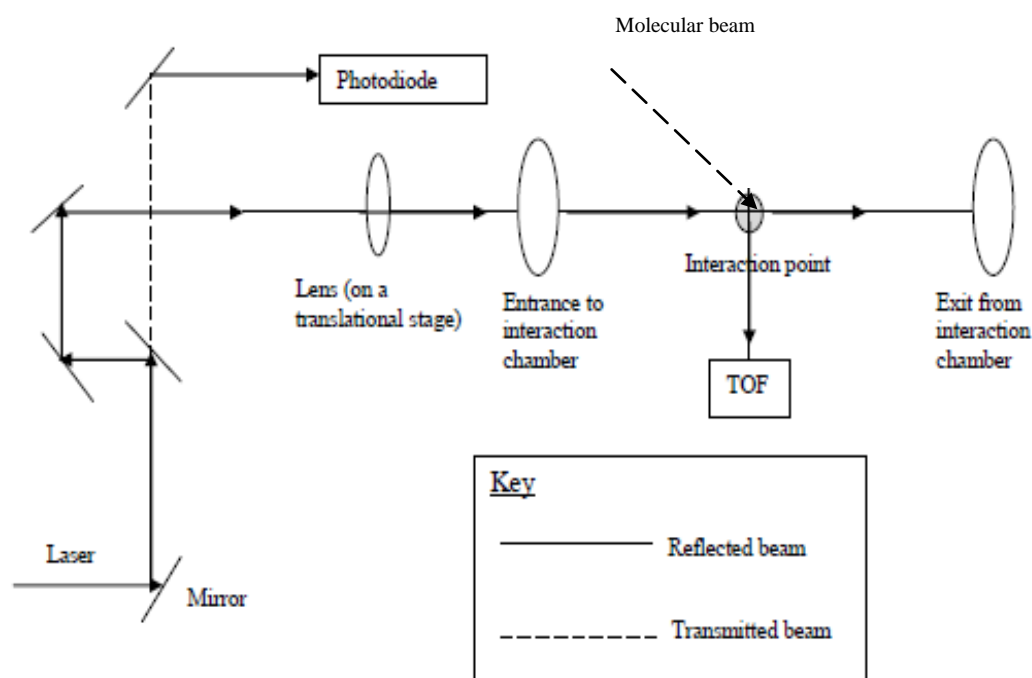


Figure 3: Birds-eye view schematic of the optical setup.

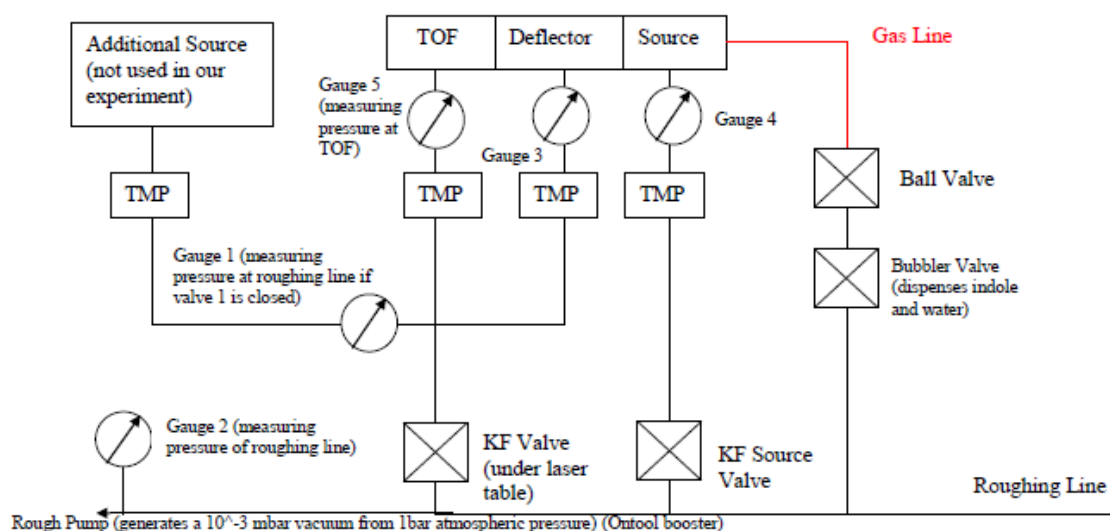


Figure 4: Schematic overview of the molecular beam setup.

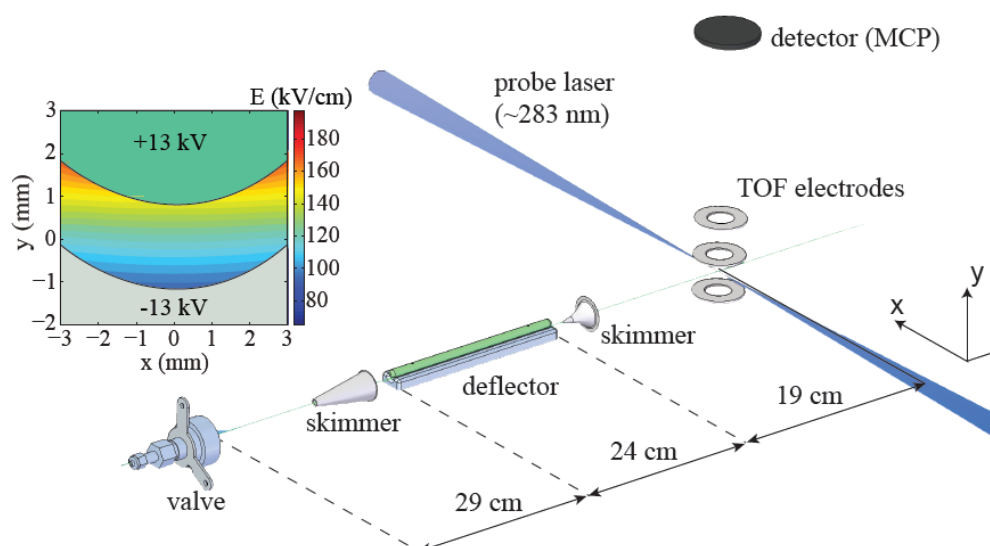


Figure 5: Schematic of the experimental setup.

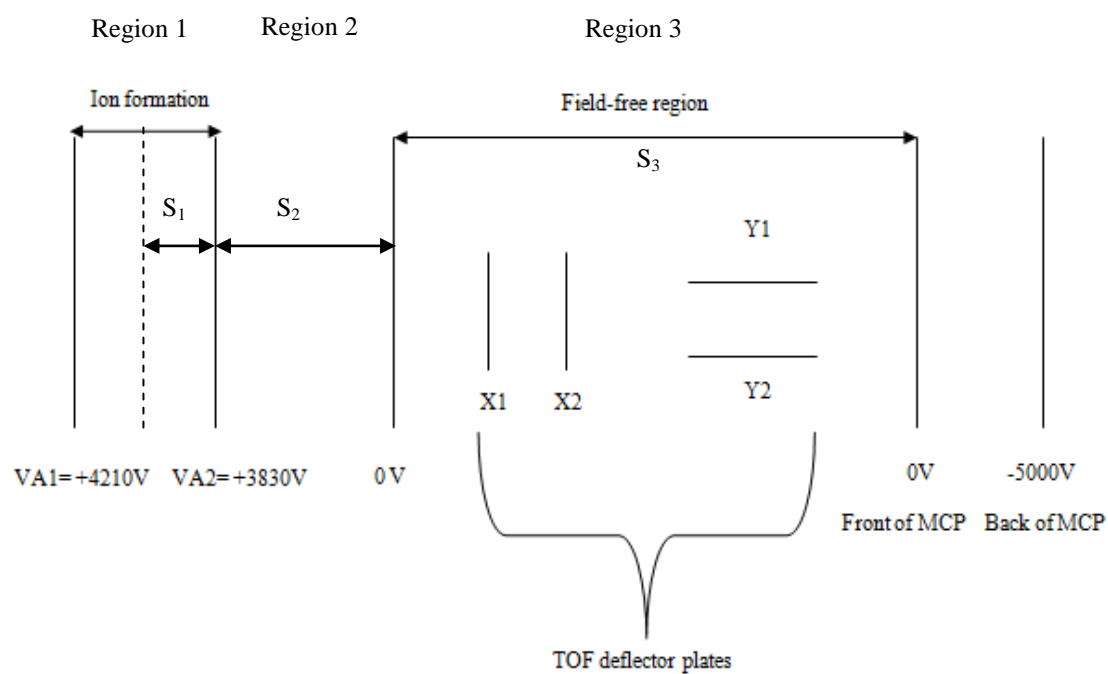


Figure 6: Interior schematic of TOF.

Experimental Deflection²

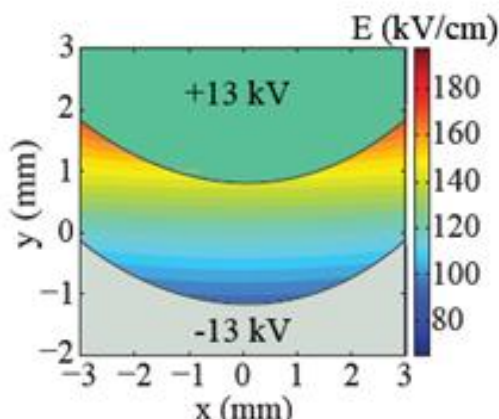


Figure 7: Cut through of the deflector, comprising of a rod and trough held at +12 kV and -12 kV respectively.

Figure 7 shows a cross section through the deflector, which is composed of a rod and trough. The rod and trough are separated by a gap, which extends to a maximum of 2.3 mm along the molecular beam axis and to a minimum of 1.9 mm close to the two electrodes. Precautions were taken to avoid dielectric breakdown at high fields, hence the maximum voltage was restricted to ± 12 kV. Coupled together, the rod and trough provide an inhomogeneous electric field, where the field is strongest in the regions close to the rod. In this setup the gradient of the electric field in the vertical direction is non-zero and the gradient in the horizontal direction equal to zero. This produces an inhomogeneous field in the vertical direction and a constant field in the horizontal direction. Since the force experienced by a polar molecule in the presence of an electric field is proportional to the gradient of the electric field, then one can see that in this experimental setup, the molecule is subject to a force in the vertical direction, thus facilitating vertical deflection.

Detection using a time-of-flight (TOF) mass spectrometer

Ion signals produced in the TOF chamber (illustrated in figure 6) are generated via photoionization of the molecular beam by the dye laser and detected via the micro channel plate (MCP). The ability to resolve the different ions produced is dependent upon the fact that although each ion should in theory be singly charged (1^+), their masses are *different*, thus allowing one to identify different ions via the detection of their mass-to-charge ratios. The lower mass ions will obtain higher speeds as they pass through the TOF chamber and will subsequently arrive at the MCP earlier as their flight times are shorter.

TOF calculations

TOF calculations were performed for each region indicated in figure 6, with the total flight time given by the sum of the flight time in each region. The flight times were calculated using simple equations of motion assuming constant linear acceleration and that the ions were formed at the midpoint between VA1 and VA2.

In region 1 the flight time was calculated using equation (1), assuming that the ions are created with zero initial velocity:

$$t_1 = \sqrt{\frac{2s_1}{\Delta V_1}} \cdot \sqrt{\frac{m}{q}} \quad (1)$$

Where ΔV_1 is the midpoint between VA1 and VA2, m is the mass of the ion and q is the charge of the ion.

The entry speed v_1 , at VA2 was calculated using equation (2):

$$v_1 = \sqrt{\frac{2\Delta V_1 q}{m}} \quad (2)$$

In region 2 the flight time was calculated using equation (3):

$$t_2 = \frac{-v_1 \pm \sqrt{v_1^2 + 2a_2 s_2}}{a_2} \quad (3)$$

Where the acceleration a_2 is given by equation (4):

$$a_2 = \frac{q\Delta V_2}{ms_2} \quad (4)$$

Where ΔV_2 is equal to the voltage at VA2.

The exit speed v_2 , from VA2 is given by equation (5):

$$v_2 = \sqrt{\frac{2q\Delta V_1}{m} + \frac{2q\Delta V_2}{m}} \quad (5)$$

The flight time in region 3 (the field-free region) is given by equation (6):

$$t_3 = \frac{s_3}{v_2} \quad (6)$$

Measurement of temporal, spatial and deflection profiles

It is observed that the detected ion signals have a finite size or width. The cause of this is attributed to an observation first discovered by Wiley and McLaren in 1955 who found that ions with the same mass-to-charge ratio exhibited a small spread in their flight times⁸. These observable effects are the repercussions of the fact that the ions contributing to the same signal will be produced at different times and locations in the field⁸. In other words, the signal shows a dependency upon the position and time at which the ions are formed, and as a result, line broadening is observed. This allows one to take temporal and spatial profiles, to see how the molecular beam varies over both time and space.

In order to measure temporal and spatial profiles, gating of the indole⁺ ion signal was performed using the Data Acquisition (DAQ) software. This entailed isolating the indole⁺ signal just before the beginning and just after the end of the signal. Thus a scan was taken over a number of intervals with each interval having between 5-10 averages, forming each point on a graph of intensity. Each point represented the mean of each of these averages. Error bars were assigned to each point by taking the standard deviation of each mean value.

Temporal profiles were produced by varying the laser delay time using the DAQ software and monitoring the variation in intensity of the indole⁺ ion signal. Spatial profiles were generated by taking spatial scans with the laser by moving the position of the lens in figure 3 and looking at how the signal intensity of the indole⁺ ion varies spatially. To obtain deflection profiles this was to be repeated at different voltage values, where the spatial profile at 0 V should give the undeflected beam and the spatial profile at the highest voltage should give the maximum deflection. Thus intensity curves could be plotted for each voltage, with the one at the highest voltage predicted to show a significant fraction of molecules deflected outside of the undeflected curve. The deflection profile would subsequently provide information of where to position an alignment laser, as the most deflected molecules are the ground/low-lying states which have the best response to laser induced alignment techniques.

Signal Location and Optimization

In order to detect an ion signal generated via laser photoionization, synchronization between the laser and the molecular beam was imperative, as the molecular beam and laser must overlap in both time and space. Rough estimates of the molecular beam's flight time from the source to the interaction point were calculated. Using the Maxwell-Boltzmann distribution for He gas at room temperature, a constant molecular beam speed of 2000 m/s was assumed. A rough measurement of the distance between the source chamber and the interaction point was made, giving an order of magnitude estimate of the molecular beam's journey distance. Simple Newtonian mechanics were employed, providing a provisional travel time of approximately 330 μ s. Thus the initial laser delay time was set to 330 μ s and it was in this manner that the signal was first identified, using a digital oscilloscope to display the signal, as illustrated in figure 8. The signal was subsequently optimized by deviating away from this time in small increments and observing the changes in intensity of the signal as shown in figure 9.

The fiducial time was determined using the photons detected at the start of the laser pulse (measured via the photodiode shown in figure 3), which impacted at the MCP and liberated electrons via the photoelectric effect. This could be seen on the MCP trace (in figure 8) as a "ringing" effect, thus flight times for the ions could be measured. The timing started when the laser reached the photodiode acting as the trigger for the experimental clock. It was assumed that the extra distance from the photodiode to the interaction point was negligible.

By modifying the laser delay time, one can alter the part of the molecular beam that is probed. If the laser beam is shot too early, then only the beginning (and less dense) part of the molecular beam pulse is seen, and conversely if the laser beam is shot too late, then only the end of the pulse is observed. The ideal case is to time the laser such that it coincides with the centre of the molecular beam, as this has the highest density of molecules and with hence create the highest signal intensity possible.

Additional calibration techniques were also employed to ensure that the maximum amount of the molecular beam reached the interaction point and was intersected by the laser beam. Referring to figure 5, the source, skimmers and deflector were mounted on motorised platforms, which were connected to a computer, thus enabling their positions to be changed accordingly when attempting to increase the signal intensity. As if either of these is offset, then the signal intensity will suffer. Also it was ensured that the laser beam was aligned along the central axis of the TOF chamber by adjusting the lens shown in figure 3.

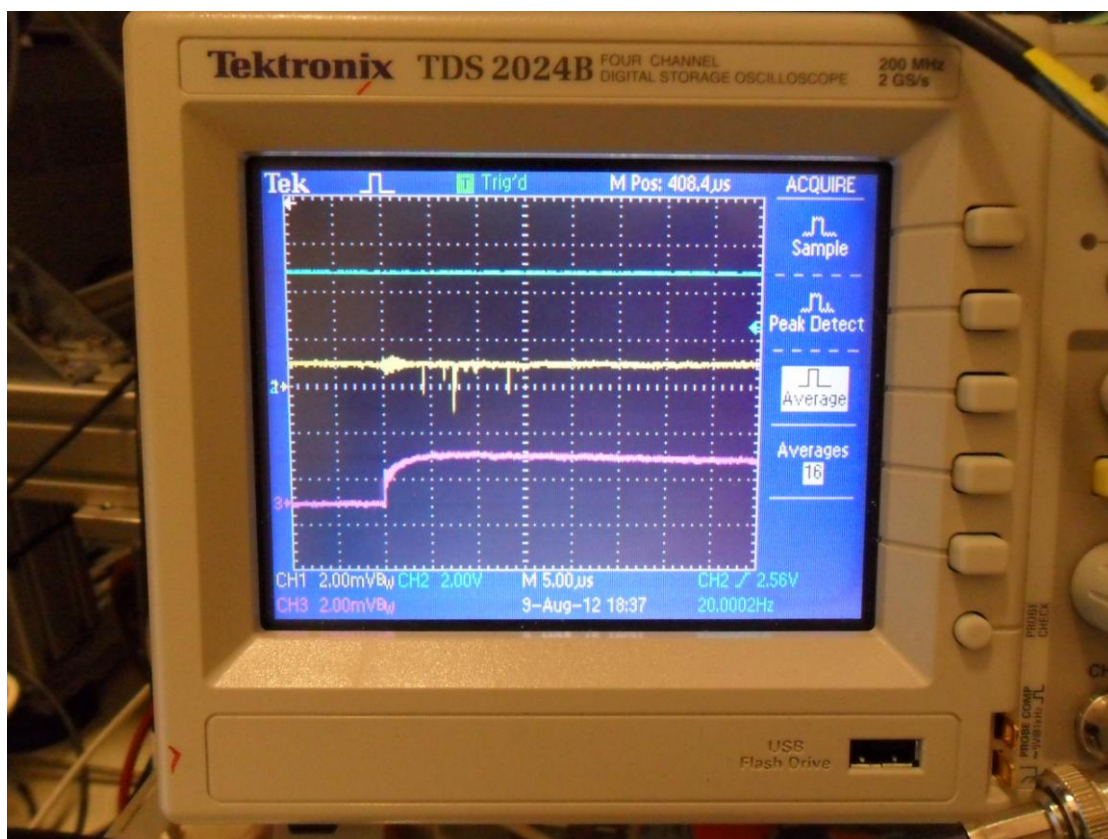


Figure 8: Scope readout showing first detection of a signal at the MCP given by the yellow trace of channel 1.

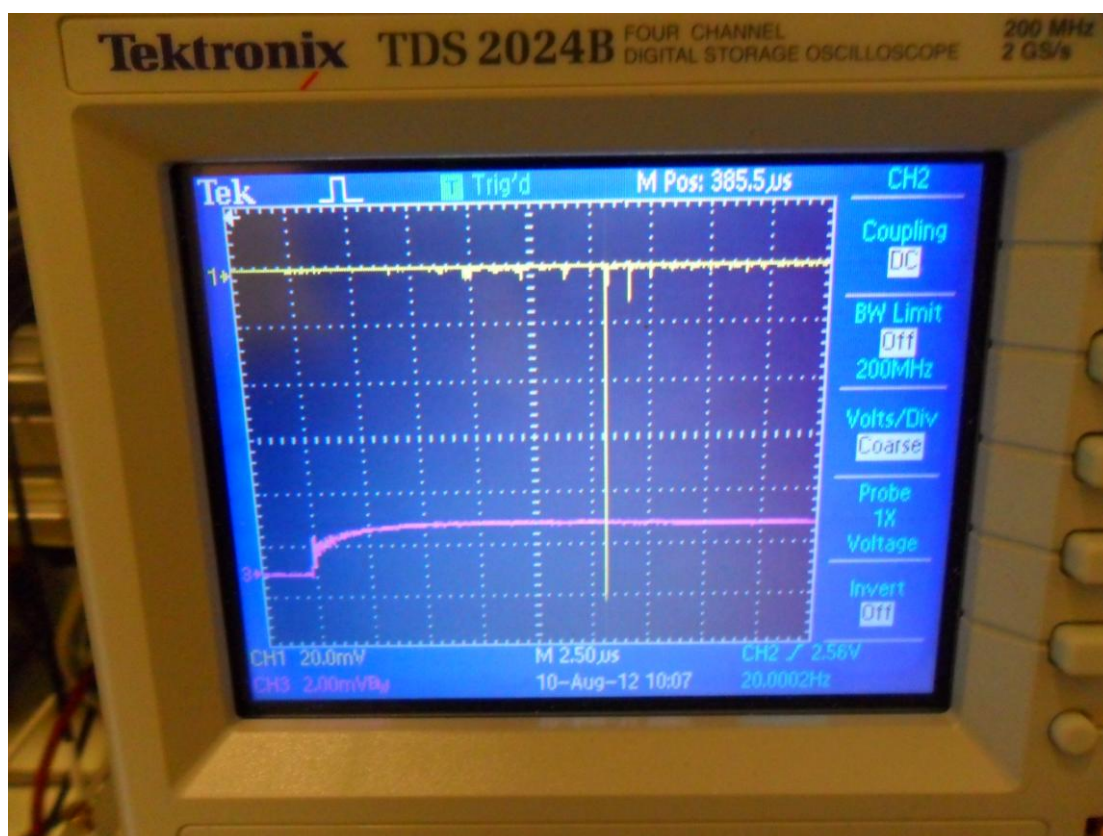


Figure 9: Scope readout showing the optimized ion signal for indole⁺.

Experimental Results and Discussion

TOF spectrums

The multiple ion signals detected at the MCP and the associated TOF and mass spectrums are shown in figures 10-15. Figures 10 and 11 show the TOF spectrum recorded with the laser at full power, with figure 11 showing a zoomed in region of the spectrum, revealing the presence of multiple peaks. The largest peak with a measured TOF of $\sim 13.69\mu\text{s}$ is attributed to indole⁺. Although the expected value from calculation was $\sim 13.03\mu\text{s}$, given that indole formed the main constituent of the sample, it is viable to assign the most prominent peak to indole⁺ with minimal uncertainty. Possible sources of error in TOF measurements could be attributed to potentially having a small offset of between 0.5 and 1 μs , (illustrated by figure 12) due to the finite speed of the photons travelling from the photodiode to the interaction point, producing a systematic shift on all ion TOFs. Additional sources of error arise from the uncertainty at which the ions are formed in both time and space, hence the distances used in the calculated times are only approximate and not absolute values, thus the calculated times are subject to error, limited by our ability to accurately measure the distances travelled. Variation of the TOFs might also be due to the presence of isotopes being detected. The subsidiary peaks to the right of the indole⁺ peak, are attributed to indole(H₂O)_n clusters (where $n=1,2,3\dots$) indicating the presence of some impurities such as water. The presence of water in the molecular beam contributes to the formation of clusters. Cluster formation imposes restrictions upon the terminal temperature attained by the molecular beam, as their formation generates heat, thus suppressing the amount of deflection observed⁵. To the left of the indole⁺ peak (as shown in figure 13), these peaks were attributed to a combination of fragmentation of the indole⁺ ion and any impurities present in the molecular beam. The presence of these additional peaks to the left of the indole⁺ peak could be due to contamination of the sample and the molecular beam, indicative of the presence of ambient air and water, whose presence also provides heating of the molecular beam, leading to an additional reduction the amount of deflection. With the laser at full power, brute-force ionization (as opposed to resonant ionization) was employed increasing the likelihood of fragmentation of the indole⁺ or indole(H₂O)_n⁺ ions and also the probability to ionize the He backing gas.

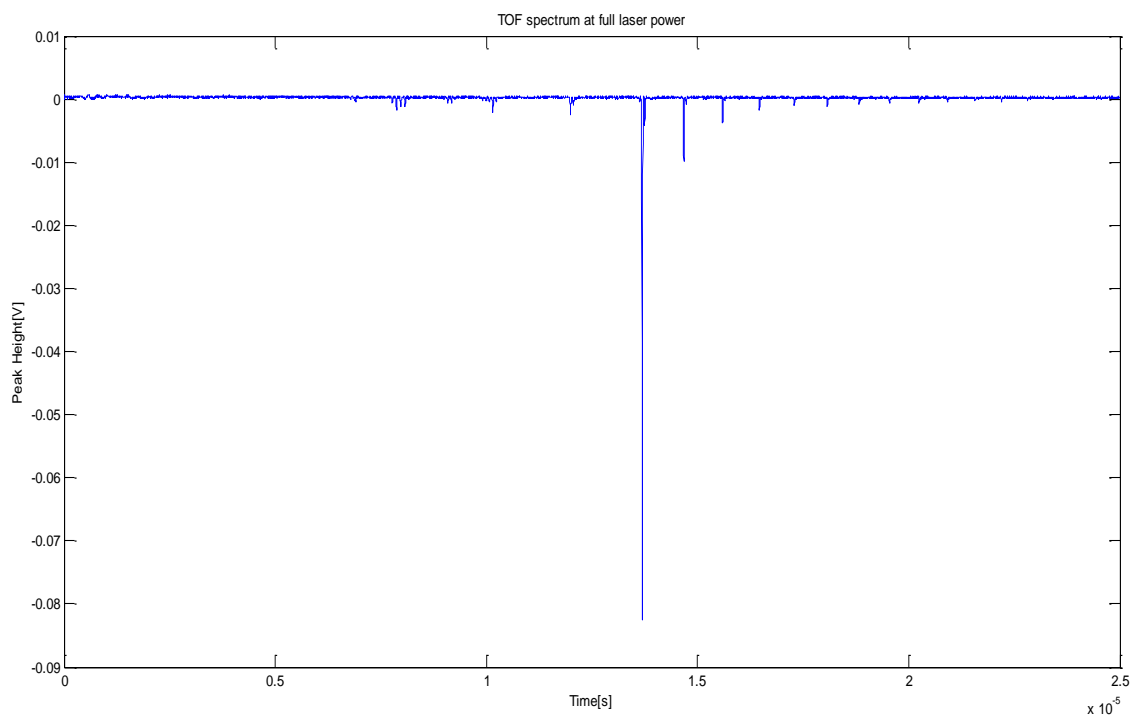


Figure 10: Graph showing the TOF spectrum at full laser power (~ 2 mJ), with flight time in 10^{-5} s on the x axis and peak height in V on the y axis.

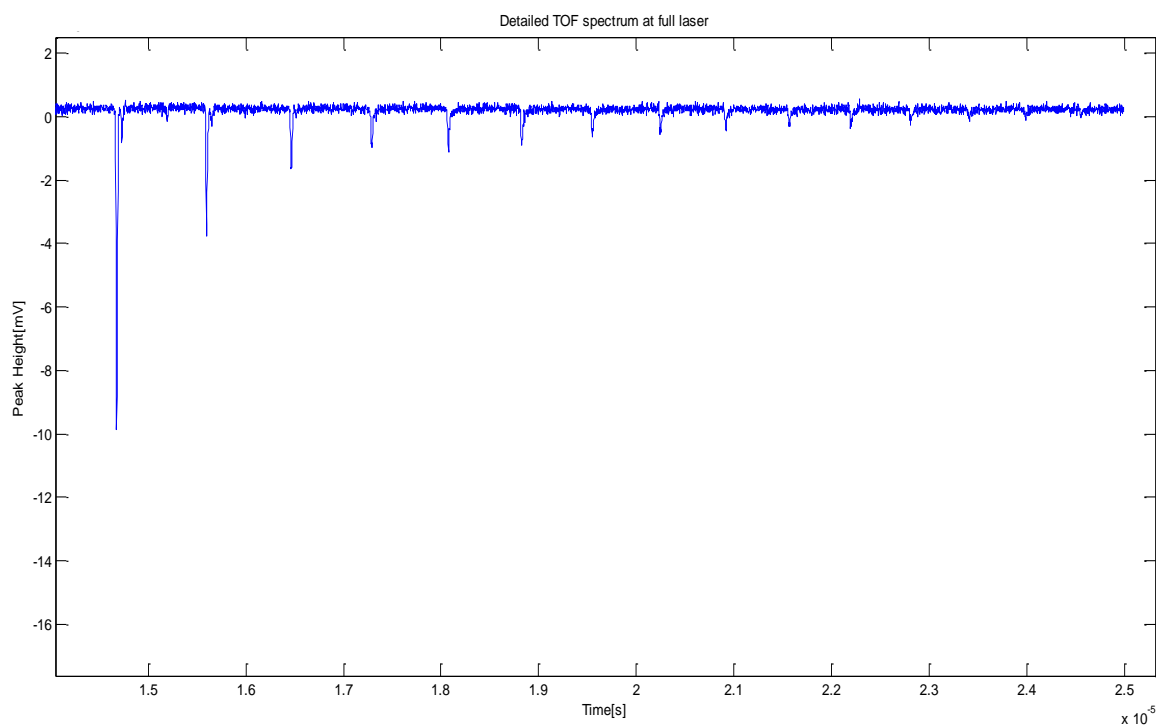


Figure 11: Graph showing the TOF spectrum at full laser power (~ 2 mJ) zoomed in over the region to the right of the indole⁺ peak illustrating water clusters. Flight time in 10^{-5} s is presented on the x axis and peak height in mV on the y axis.

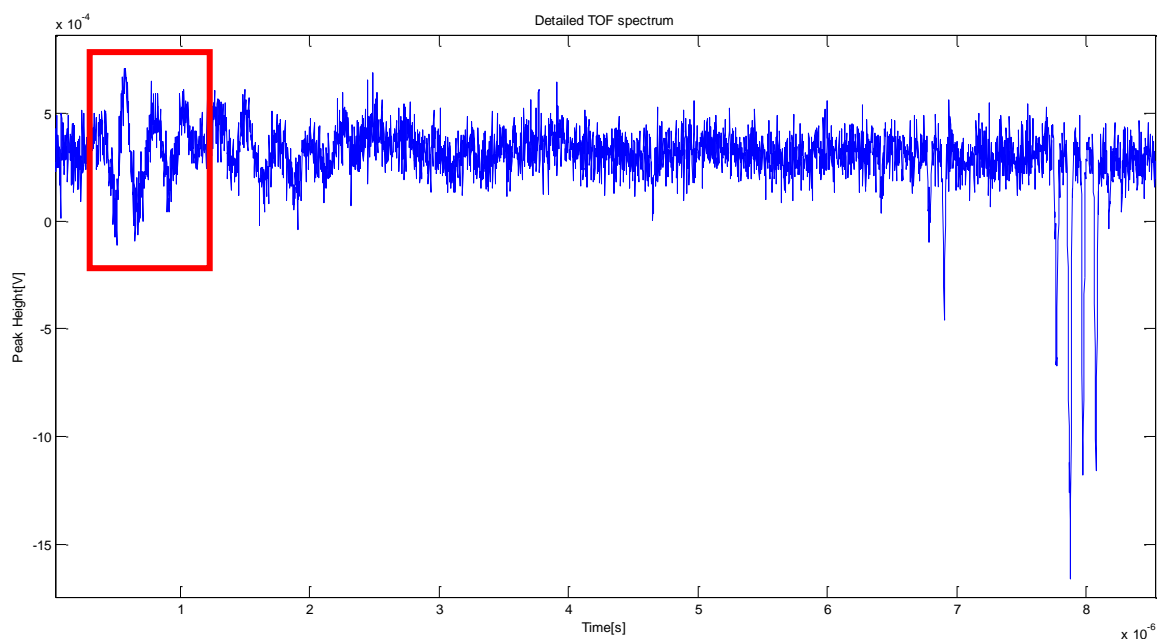


Figure 12: Graph showing the TOF spectrum at full laser power ($\sim 2\text{mJ}$) zoomed in over the region to the right of the indole⁺ peak illustrating a possible source of an offset. Flight time in 10^{-6} s is presented on the x axis and peak height in 10^{-4} V on the y axis. The red box indicates the region for the potential location of the offset.

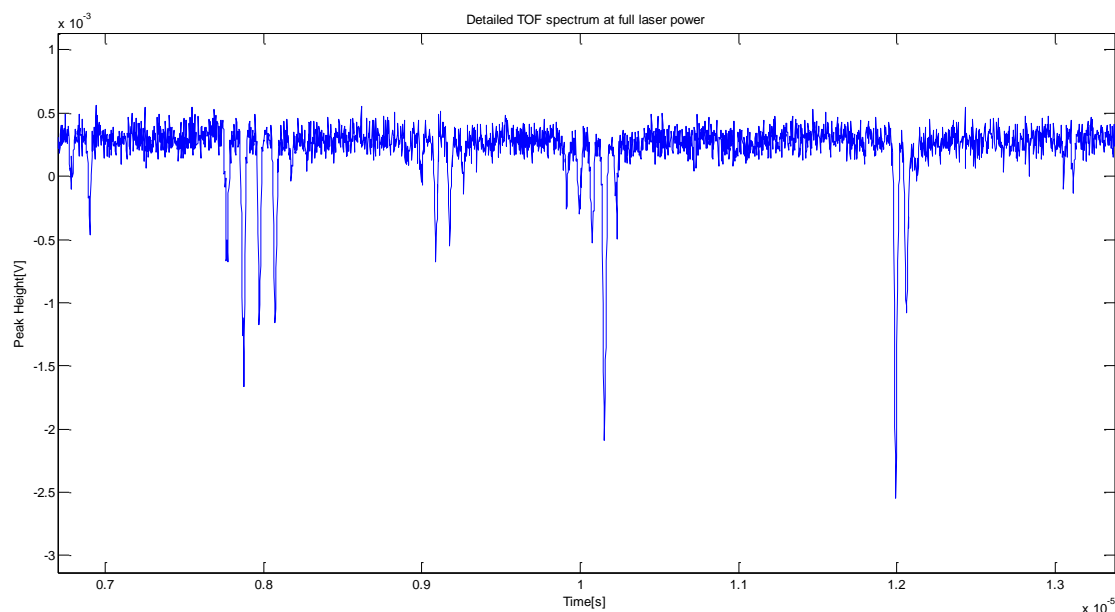


Figure 13: Graph showing the TOF spectrum at full laser power ($\sim 2\text{mJ}$) zoomed in over the region to the left of the indole⁺ peak illustrating fragments and impurities present. Flight time in 10^{-5} s is presented on the x axis and peak height in 10^{-3} V on the y axis.

Assuming singly charged ions, then the time axis in figure 10 can be converted to a mass axis to produce a mass spectrum as shown in figure 14.

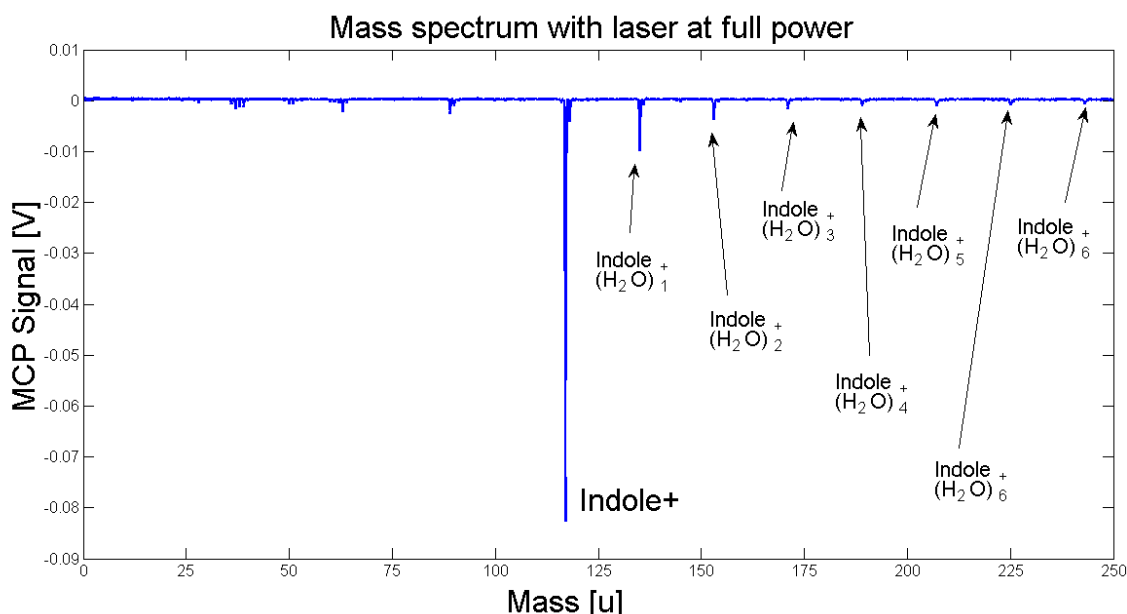


Figure 14: Graph showing the mass spectrum at full laser power ($\sim 2\text{mJ}$) after rinsing of the gasline. Mass in atomic mass units is presented on the x axis and MCP signal in V on the y axis. The indole and indole water peaks are labelled.

Cluster formation and contamination within the molecular beam were not desirable; hence the gasline was rinsed thoroughly to remove any traces of water molecules or contamination of the backing gas with nitrogen or oxygen. After this procedure, another TOF spectrum was recorded as illustrated by figure 15, showing a significant reduction in the number of clusters (to the right of the indole⁺ peak) and impurities (to the left of the indole⁺ peak). The lack of cluster suggests a cold beam, which is crucial for deflection. Also the rinsing of the gasline would improve deflection, as the presence of ambient air leads to a reduction in the speed of the molecular beam, since the speed is set by the mass of the backing gas⁵. Hence a slow beam, implies a warmer beam and thus the sample is not in the rotational ground/low-lying states, resulting in poor deflection.

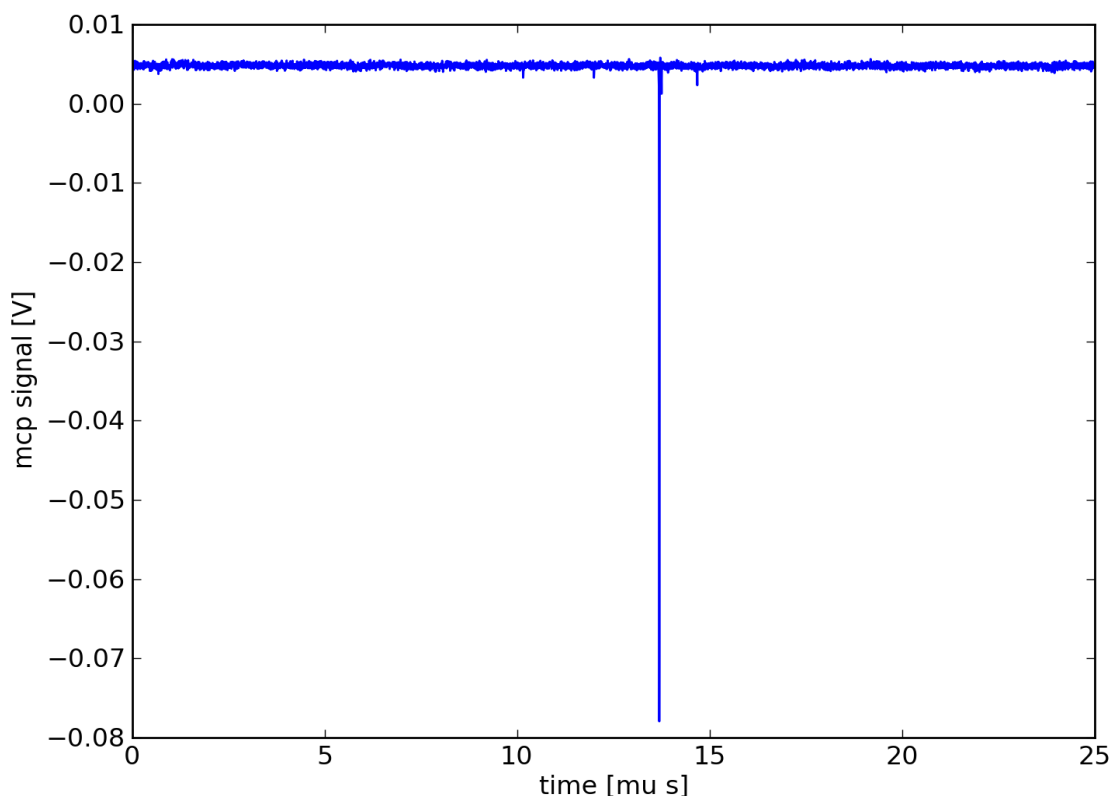


Figure 15: Graph showing the TOF spectrum at full laser power ($\sim 2\text{mJ}$) after rinsing of the gasoline. Flight time in μs is presented on the x axis and MCP signal in V on the y axis.

Temporal Profiles

Temporal profiles of the molecular beam were taken with varying opening times of the E-L valve. Ideally, an E-L valve opening time, which gave a small molecular beam pulse width was preferable. However, the cooling of the beam was improved by having a longer E-L valve opening time, which ensured better deflection, thus an E-L valve opening time of $10\mu\text{s}$ was chosen as a compromise between a narrow temporal beam profile and cool molecular beam as shown in figure 16.

Figure 16 was used to decide on an optimum laser delay time. The arrow marks the time, ($392\mu\text{s}$), where the laser delay was set in order to obtain good deflection. It was chosen to shoot the laser off-peak, as the earlier parts of the molecular beam, should be the coldest. Thus $392\mu\text{s}$ was chosen, as although the signal intensity would be weaker as at this time since the laser would be probing the pulse in a region containing a lower density of molecules, it should be cooler, thus ensuring better deflection.

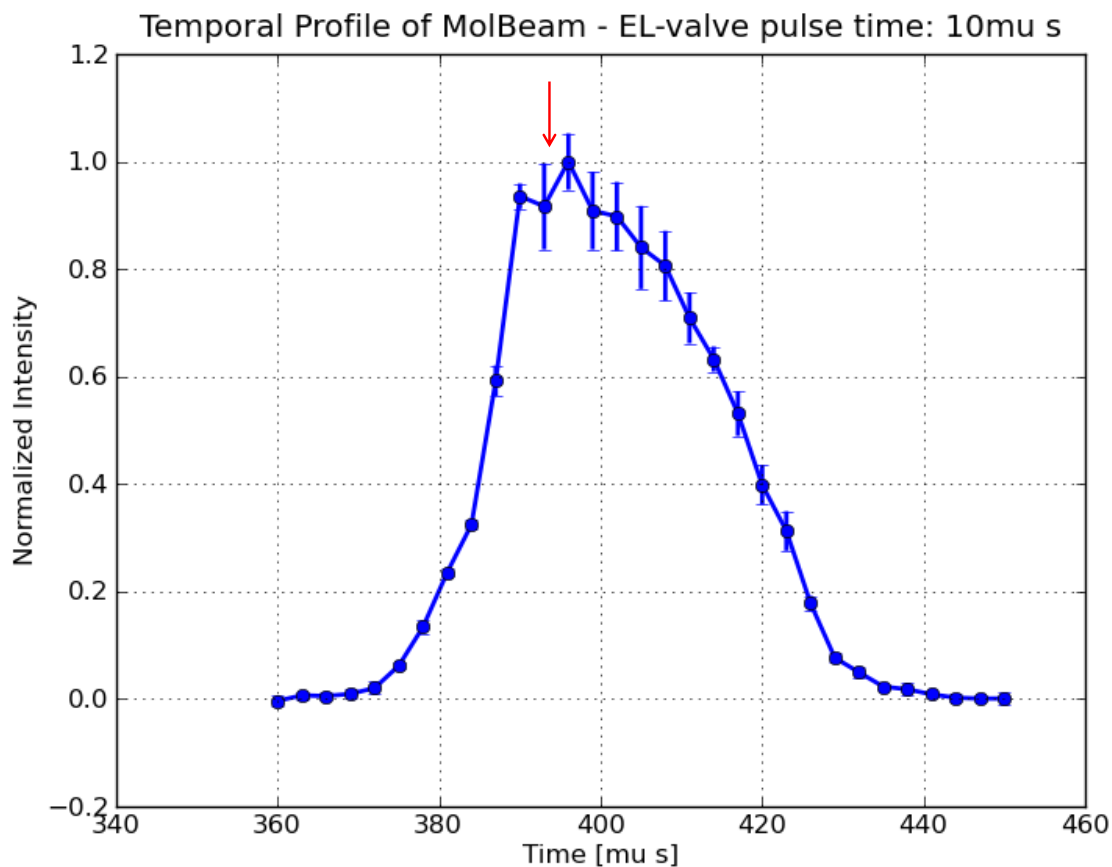


Figure 16: Graph showing the temporal profile of the molecular beam at an EL valve pulse time of 10 μ s.

Deflection Optimization

In order to optimize deflection, it was imperative to re-align the molecular beam, as once the deflector is applied, the molecular beam will be deviated away from its original path. Also laser delay times were varied to ensure the best deflection. Thus the optimum settings were determined, allowing the greatest amount of deflection to be observed.

Deflection profiles

Figure 17 shows the deviation of the molecular beam's path with various deflector voltages, in accordance with the deflection theory. From figure 17 a maximum deflection of ~ 1.2 mm at ± 12 kV is estimated. The greater the electric field applied, the greater the interaction, hence the larger the deflection one sees. Thus figure 17 illustrates that neutral polar molecules in the gaseous phase can be successfully deflected and thus spatially separated into different quantum states, via the action of an inhomogeneous electric field.

Figure 17 shows deflection towards the left, which in this setup corresponds to deflection towards the rod, away from the trough. The deflection obtained is greatest at the highest voltage applied (i.e. the cyan curve), with the region indicated by the arrow showing complete separation between the deflected and undeflected molecules. Thus this region would exhibit the greatest susceptibility to laser induced alignment. This is indicative of spatial separation of the quantum states for indole molecules, with figure 17 showing the generation of state-selected states. If one assumes that the undeflected indole profile (given by the blue curve) is the same as for He, since He is non-polar and thus should show no deflection, then separation between the sample and backing gas can be achieved. The ability to spatially separate He and indole is important, as the samples produced are to form targets for future diffraction experiments, where the presence of any He would cause blurring to the diffraction image, limiting the amount of detail which can be resolved about the molecule's structure.

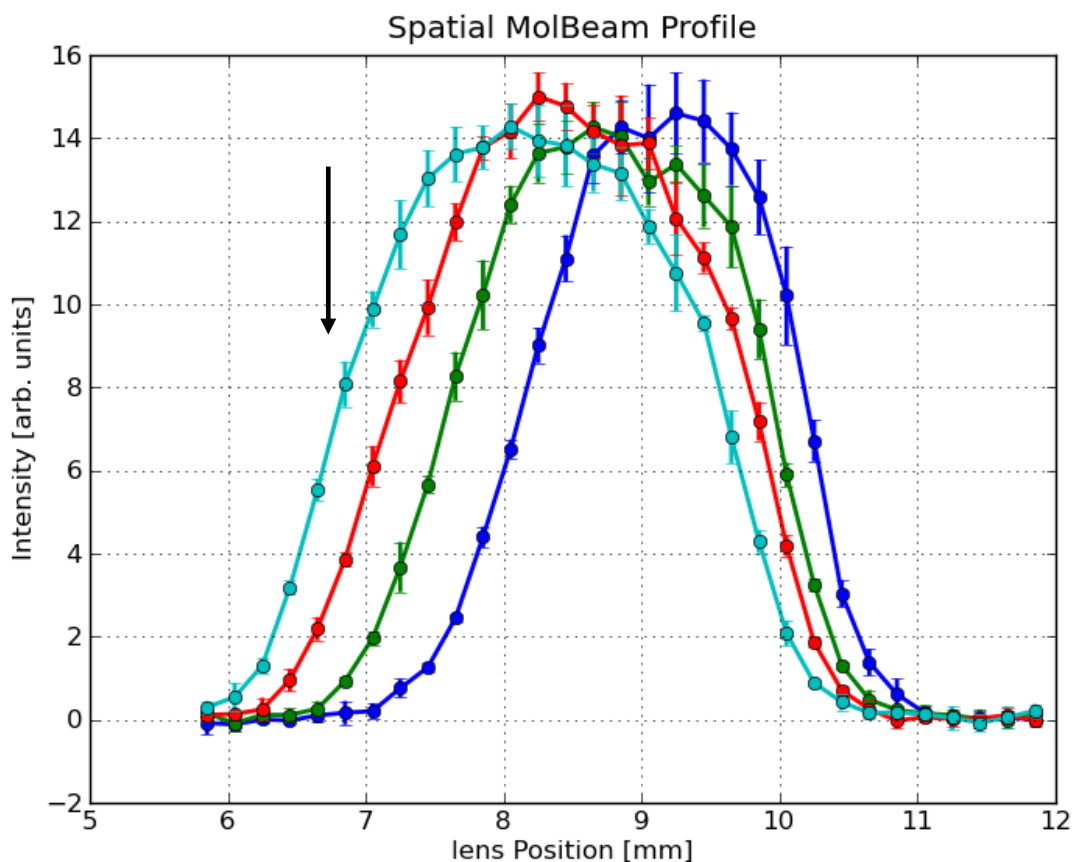


Figure 17: Graph showing spatial profiles at various deflector voltages. The blue curve is the spatial profile for the undeflected beam, with the deflector off. The green curve is the deflection profile for the beam with the deflector held at ± 6 kV. The red curve is the deflection profile obtained at ± 9 kV. The cyan curve is the deflection profile acquired at ± 12 kV.

Conclusion

Deflection profiles were obtained for a gaseous molecular sample of indole via exploitation of the polar molecule's dipole moment in an inhomogeneous electric field. The results demonstrate that one can use the principle of deflection in order to generate spatially separated low-lying quantum states. The importance of this experiment is that the state-selected samples produced provide hope for further experiments such as the goal of diffraction of single molecules in the gaseous phase. Here the state-selected samples pose as ideal targets for laser induced alignment experiments, leading ultimately towards diffraction of gaseous molecular samples.

Acknowledgments

I would like to thank everyone in the CMI group for giving me a fantastic opportunity and for allowing me to experience what it is like to be part of a research group. I will come away from this programme with knowledge in an area of physical research that I might otherwise have never come across.

References

1. A.C. Philips., *Introduction to Quantum Mechanics*, Wiley.
2. F. Filsinger et al., *Quantum-state selection, alignment, and orientation of large molecules using static electric and laser fields*, *J. Chem. Phys.* **131**, 064309 (2009).
3. W. Demtroder., *Molecular Physics*, Wiley.
4. S. Trippel et al., *Spatial separation of state and size selected neutral clusters* arXiv: 1208.4935v1 (2012).
5. R. Schäfer., P. Schmidt., *Methods in Physical Chemistry*, Chapter 1, Wiley-VCH.
6. Y-J. Wu., *New Indole-Containing Medicinal Compounds*, *Top Heterocycl Chem* (2010) **26**: 1–29 DOI: 10.1007/7081_2010_37, ©Springer-Verlag Berlin Heidelberg 2010.
7. Image from: <http://en.wikipedia.org/wiki/Indole> Date accessed: 27/08/12.
8. www.jic.ac.uk/services/proteomics/tof.htm Date accessed: 16/08/12.